Loss of Rbm24a causes defective hair cell development in the zebrafish inner ear and neuromasts

Xiao-Ning Cheng, Jing-Jing Zhang, De-Li Shi

Letter to the Editor

Loss of Rbm24 causes defective hair cell development in the zebrafish inner ear and neuromasts

Zebrafish presents many advantages for the study of hair cell differentiation, and has become particularly attractive for understanding the development of vertebrate sensory organs. During the past decades, mutagenesis screening in this model has allowed the identification of a large number of genes implicated in otic development, some of which were associated with human diseases affecting hearing function (Blanco-Sánchez et al. 2017; Nicolson, 2017). These genes essentially encode components of key signaling pathways, transcription factors, or structural constituents. Functional analyses have contributed to our understanding on the transcriptional control of otic placode specification and differentiation (Nicholson, 2017). However, the posttranscriptional mechanism underlying hair cell differentiation and function remains largely elusive, mostly due to lack of mutations affecting related regulatory networks. RNA-binding proteins (RBPs) are implicated in posttranscriptional regulation of gene expression in development and disease (Brinegar and Cooper, 2016). Rbm24 exhibits strongly localized and highly conserved expression pattern in all vertebrate embryos (Grifone et al. 2014, 2018). Beside its expression and implication in skeletal and cardiac muscle development (Li et al. 2010; Poon et al. 2012; Grifone et al. 2014; Maragh et al. 2014; Yang et al. 2014), it is also expressed in a subset of cells within the differentiating head sensory organs. Particularly, Rbm24 protein co-localizes in the cytoplasm with Myo7A in inner and outer cells of the cochlea, as well as in the saccular and utricular maculae, and in semicircular canals of the mouse early embryo (Grifone et al. 2018). This implies that Rbm24 may posttranscriptionally regulate hair cell development and function, but no functional evidence has been reported in vertebrates.

Zebrafish genome contains two *rbm24* paralogs, *rbm24a* and *rbm24b*. The expression pattern of *rbm24a* in different tissues is identical as that of *rbm24* in other vertebrates. From previous works (Poon et al. 2012; Maragh et al. 2014), it can be observed that only *rbm24a* is expressed in the otic vesicle during early stages of development, whereas *rbm24b* does not show

such an expression pattern. We have generated a zebrafish *rbm24a* mutant line by TALEN-mediated genome-editing approach (Shao et al. 2020). Heterozygous mutants developed normally, whereas homozygous mutants showed specific loss of function phenotypes, which could be readily distinguished by the appearance of heart edema at 1.5 dpf (days postfertilization) onward, and verified by allele-specific PCR (Fig. S1). Examination of the otic phenotype revealed a progressive occurrence of otic development defects in *rbm24a* mutants, which were evident at 3 dpf, and characterized by a delayed fusion of semicircular canals in a majority of embryos (arrow in Fig. 1A). In addition, the size of otic vesicles in *rbm24a* mutants was reduced as development proceeds, but the semicircular canals eventually fused at 4 dpf (Fig. S2). Analyses of the startle response indicated that *rbm24a* mutant larvae were largely unresponsive to acoustic stimulation (Fig. 1B, C), and displayed balancing deficits. These observations suggest that mutation of *rbm24a* impairs otic development and causes hearing and balance deficits.

To analyze how loss of Rbm24a function affects otic neural development, we first examined the expression of several representative markers of the otic vesicle by in situ hybridization. The expression of *sox2*, which specifies sensory fates in the otic vesicle (Gou et al. 2018), was not affected in *rbm24a* mutants (Fig. S3A). The expression patterns of two crista markers, *fgf10a* and *msx3* (Thisse and Thisse, 2004), were also unchanged in *rbm24a* mutants, despite an obviously reduced size of the otic vesicle (Fig. S3B, C). These results suggest that Rbm24a should function downstream of these factors, and may be not involved in the specification of the otic vesicle. However, the expression of *myo7a*, which localizes to sensory hair cells when these cells start the differentiation, and is required for hair bundle integrity (Ernest et al. 2000), was obviously reduced in the otic vesicle and in different neuromasts in the mutants at 3 dpf (Fig. 1D). This implies that loss of Rbm24a should affect the differentiation of hair cells. We thus addressed this question more precisely using the *Tg(pou4f3:GAP-GFP)* transgene (Xiao et al. 2005). At 3 dpf, *rbm24a* mutants exhibited strongly reduced fluorescence intensity both in the otic vesicle and in the posterior lateral line system (Fig. 1E). Examination of the first five neuromasts (L1-L5), without taking into account the differences in fluorescence intensity, revealed that their number was reduced in *rbm24a* mutants (Fig. 1F). In general, the fifth neuromast (L5) could be observed

in a few mutant embryos, and the most posterior neuromasts (L6 and L7) were generally not observed in the mutant embryos. This result suggests that the formation of hair cells in the otic vesicle and the deposition of neuromasts are defective following loss of Rbm24a function.

It remains to be determined how hair cell differentiation in different positions is affected in *rbm24a* mutants. We set to examine in more detail the formation and organization of hair cells in the otic vesicle and in the first three neuromasts of the posterior lateral line system (Fig. 1G). The size of the three cristae (anterior, lateral and posterior cristae) seemed to be reduced in *rbm24a* mutants. Since each hair cell within the crista forms one kinocilium that is more accessible for observation, we used this criterion to monitor the defects of hair cell development. This could reflect to some extent the number of hair cells in each crista. Statistical analyses showed a significantly reduced number of kinocilia in the three cristae (Fig. 1H). The height of these kinocilia was also reduced to some extent, particularly in the lateral crista. In the utricular macula of *rbm24a* mutants, hair cells were not properly aligned, and cell extruding could be observed in a large majority of embryos (Fig. 1G, I). Similar defects have been observed in *sox2* morphants with defective maintenance and regeneration of hair cells (Millimaki et al. 2010). Due to the difficulty to observe saccular macula, we did not detect obvious differences in the cellular organization between WT sibling and *rbm24a* mutants. In the first three neuromasts that we examined, the cellular organization into rosette was severely disrupted in *rbm24a* mutants, which was correlated with a reduced number of hair cells (Fig. 1G, J). These phenotypic and quantitative analyses clearly demonstrate that hair cell development is defective in *rbm24a* mutants, and they are consistent with the expression of vertebrate Rbm24 in the cristae and maculae (Grifone et al. 2018). At present, it is not clear whether Rbm24a is expressed in neuromasts, and thus how its mutation affects neuromast hair cells. We thus performed in situ hybridization to examine more precisely the expression sites of *rbm24a* at 1 dpf. This revealed that *rbm24a* transcripts were also localized in the posterior lateral line primordium (pLLP), in addition to anterior and posterior cristae (Fig. 1K). The pLLP forms from the otic vesicle and migrates caudally to periodically deposit neuromasts (Chitnis et al. 2012). Thus, the expression of *rbm24a* in this placode may explain the defects of neuromast hair cell development in *rbm24a*

mutants.

We thus demonstrated for the first time that loss of Rbm24a affected hair cell formation and organization. Both zebrafish *rbm24a* and mouse Rbm24 show dynamic expression during hair cell differentiation (Grifone et al. 2018; Lush et al. 2019), and it may function downstream of transcription factors, such as Atoh1, in hair cell development and regeneration (Cai et al. 2015). Indeed, it is of interest to note that loss of Rbm24a function has no effect on the expression of several genes coding for transcription factors that are involved in otic vesicle specification, but it affects the expression of hair cell differentiation genes, such *myo7a*. This is fully consistent with our recent finding showing that Rbm24 protein is localized in the cells where Myo7A is expressed (Grifone et al. 2018), and raises the question whether and how Rbm24a posttranscriptionally regulates *myo7a* whose dysfunction causes the Usher syndrome type 1B (Weil et al. 1995). Besides the specific otic phenotype, our observation of *rbm24a* expression in the pLLP is also of interest for understanding the developmental mechanisms of vertebrate sensory systems, because the advantages of the zebrafish posterior lateral line system (Ghysen and Dambly-Chaudière, 2007). Thus, this work could not only provide a useful model to study hearing disorders, it also should open novel avenues for investigating posttranscriptional control in these processes. Along with our present findings demonstrating a critical role of Rbm24 in regulating cytoplasmic polyadenylation during lens differentiation (Shao et al. 2020), the present work further emphasizes a critical role of posttranscriptional regulation in the development of head sensory organs. Given the importance of RBPs in development and diseases, and the highly conserved expression of vertebrate Rbm24 in hair cells, it will be particularly interesting to identify human mutations affecting the *cis*-regulatory elements that disrupt its inner ear specific expression and lead to hearing disorders.

Acknowledgments

We thank Y.F. Feng for assistance with startle response test and hair cell analysis. This work was supported by the National Key R&D Project of China (grant number 2018YFA0801000), the National Natural Science Foundation of China (grant numbers 31671509, 31900577), the Centre

National de la Recherche Scientifique (CNRS), and the Sorbonne University.

References

Blanco-Sánchez, B., Clément, A., Phillips, J.B., Westerfield, M., 2017. Zebrafish models of human eye and inner ear diseases. Methods Cell Biol. 138, 415-467. https://doi.org/10.1016/bs.mcb.2016.10.006.

Brinegar, A.E., Cooper, T.A., 2016. Roles for RNA-binding proteins in development and disease. Brain Res. 1647, 1-8. https://doi.org/10.1016/j.brainres.2016.02.050.

Cai, T., Jen, H.I., Kang, H., Klisch, T.J., Zoghbi, H.Y., Groves, A.K., 2015. Characterization of the transcriptome of nascent hair cells and identification of direct targets of the Atoh1 transcription factor. J. Neurosci. 35, 5870-5883. https://doi.org/10.1523/JNEUROSCI.5083-14.2015.

Chitnis, A.B., Nogare, D.D., Matruda, M., 2012. Building the posterior lateral line system in zebrafish. Dev. Neurobiol. 72, 234-255. https://doi.org/10.1002/dneu.20962.

Ernest, S., Rauch, G.J., Haffter, P., Geisler, R., Petit, C., Nicolson, T., 2000. Mariner is defective in myosin VIIA: a zebrafish model for human hereditary deafness. Hum. Mol. Genet. 9, 2189-2196. https://doi.org/10.1093/hmg/9.14.2189.

Ghysen, A., Dambly-Chaudière, C., 2007. The lateral line microcosmos. Genes Dev. 21, 2118-2130. https://doi.org/10.1101/gad.1568407.

Gou, Y., Vemaraju, S., Sweet, E.M., Kwon, H.J., Riley, B.B., 2018. sox2 and sox3 play unique roles in development of hair cells and neurons in the zebrafish inner ear. Dev. Biol. 435, 73-83. https://doi.org/10.1016/j.ydbio.2018.01.010.

Grifone, R., Xie, X., Bourgeois, A., Saquet, A., Duprez, D., Shi, D.L., 2014. The RNA-binding protein Rbm24 is transiently expressed in myoblasts and is required for myogenic differentiation during vertebrate development. Mech. Dev. 134, 1-15. https://doi.org/10.1016/j.mod.2014.08.003.

Grifone, R., Saquet, A., Xu, Z., Shi, D.L., 2018. Expression patterns of Rbm24 in lens, nasal epithelium, and inner ear during mouse embryonic development. Dev. Dyn. 247, 1160-1169. https://doi.org/10.1002/dvdy.24666.

Li, H.Y., Bourdelas, A., Carron, C., Shi, D.L., 2010. The RNA-binding protein Seb4/RBM24 is a direct target of MyoD and is required for myogenesis during Xenopus early development. Mech. Dev. 127, 281-291. https://doi.org/10.1016/j.mod.2010.03.002.

Lush, M.E., Diaz, D.C., Koenecke, N., Baek, S., Boldt, H., St Peter, M.K., Gaitan-Escudero, T., Romero-Carvajal, A., Busch-Nentwich, E.M., Perera, A.G., Hall, K.E., Peak, A., Haug, J.S., Piotrowski, T., 2019. scRNA-Seq reveals distinct stem cell populations that drive hair cell regeneration after loss of Fgf and Notch signaling. Elife. 8, pii:e44431. https://doi.org/10.7554/eLife.44431.

Poon, K.L., Tan, K.T., Wei, Y.Y., Ng, C.P., Colman, A., Korzh, V., Xu, X.Q., 2012. RNA-binding protein RBM24 is required for sarcomere assembly and heart contractility. Cardiovasc. Res. 94, 418-427. https://doi.org/10.1093/cvr/cvs095.

Maragh, S., Miller, R.A., Bessling, S.L., Wang, G., Hook, P.W., McCallion, A.S., 2014. Rbm24a and Rbm24b are required for normal somitogenesis. PloS One 9, e105460. https://doi.org/10.1371/journal.pone.0105460.

Millimaki, B.B., Sweet, E.M., Riley, B.B., 2010. Sox2 is required for maintenance and regeneration, but not initial development, of hair cells in the zebrafish inner ear. Dev. Biol. 338, 262-269. https://doi.org/10.1016/j.ydbio.2009.12.011.

Nicolson, T., 2017. The genetics of hair-cell function in zebrafish. J. Neurogenet. 31, 102-112. https://doi.org/10.1080/01677063.2017.1342246.

Shao, M., Lu, T., Zhang, C., Zhang, Y.Z., Kong, S.H., Shi, D.L., 2020. Rbm24 controls poly(A) tail length and translation efficiency of crystallin mRNAs in the lens via cytoplasmic polyadenylation. Proc. Natl. Acad. Sci. U. S. A. (in press).

Thisse, B., Thisse, C., 2004. Fast Release Clones: A High Throughput Expression Analysis. ZFIN Direct Data Submission (http://zfin.org).

Weil, D., Blanchard, S., Kaplan, J., Guilford, P., Gibson, F., Walsh, J., Mburu, P., Varela, A., Levilliers, J., Weston, M.D., Kelley, P.M., Kimberling, W.J., Wagenaar, M., Levi-Acobas, F., Larget-Piet, D., Munnich, A., Steel, K.P., Brown S.D.M, Petit, C., 1995. Defective myosin VIIA gene responsible for Usher syndrome type 1B. Nature 374, 60-61. https://doi.org/10.1038/374060a0.

Xiao, T., Roeser, T., Staub, W., Baier, H., 2005. A GFP-based genetic screen reveals mutations that disrupt the architecture of the zebrafish retinotectal projection. Development 132, 2955-2967. https://doi.org/10.1242/dev.01861.

Yang, J., Hung, L.H., Licht, T., Kostin, S., Looso, M., Khrameeva, E., Bindereif, A., Schneider, A., Braun, T., 2014. RBM24 is a major regulator of muscle-specific alternative splicing. Dev. Cell 31, 87-99. https://doi.org/10.1016/j.devcel.2014.08.025.

Author information

Xiao-Ning Cheng[1], Jing-Jing Zhang[1] and De-Li Shi[1,2]*

[1]Affiliated Hospital of Guangdong Medical University, Zhanjiang 524001, China

[2]Develompental Biology Laboratory, CNRS UMR7622, Institut de Biologie Paris-Seine, Sorbonne University, 75005 Paris, France

*Corresponding author

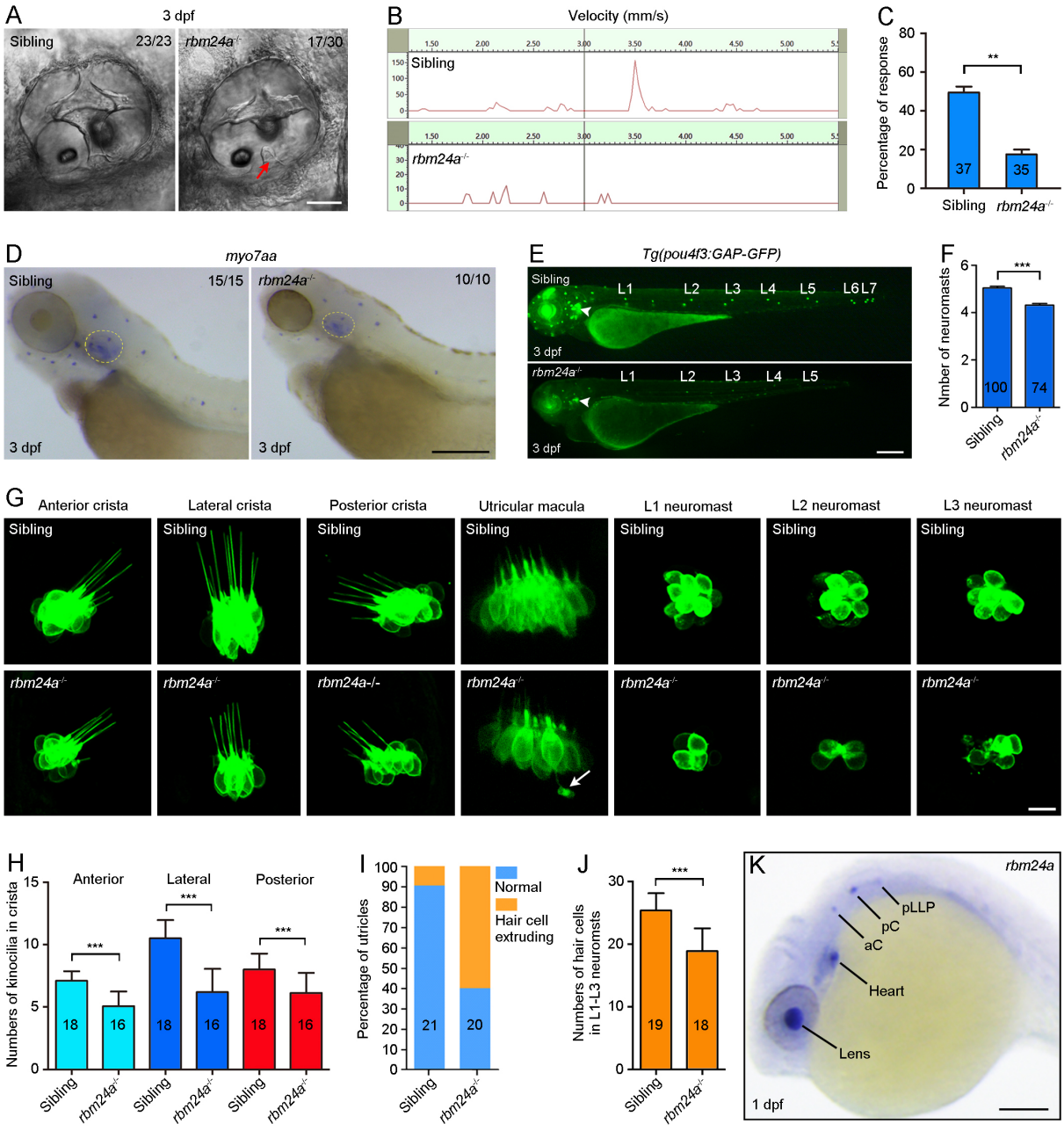

Fig.1. Defective hair cell development in zebrafish *rbm24a* mutants. **A**: Confocal differential interference contrast images extracted from Fig. S2 show otic phenotypes at 3 dpf. Notice the delayed fusion of semicircular canals in *rbm24a* mutants (red arrow). Scale bar: 50 μm. **B**: Representative graphs from startle response test compare the behaviors of WT siblings and *rbm24a* mutants at 3 dpf. **C**: Statistical analyses of the responses to acoustic stimulation. The number in each column indicates total embryos tested in three independent experiments (**, $p < 0.01$; Student's *t*-test). **D**: In situ hybridization analysis shows the reduced expression of *myo7aa* in the otic vesicle (outline by yellow circle) and neuromasts in *rbm24a* mutants at 3 dpf. Scale

bar: 25 μm. **E**: Defective development of the otic vesicle (arrow) and neuromasts (L1 to L5) in *rbm24a* mutants at 3 dpf, as revealed by the *Tg(pou4f3:GAP-GFP)* transgene. Scale bar: 10 μm. **F**: Statistical analyses compare the formation of the first five neuromasts between WT siblings and *rbm24a* mutants. The differences in fluorescence intensity were not taken into account, and the results were obtained three independent batches, with total numbers of embryos indicated in the columns (***, $p < 0.001$; Student's *t*-test). **G**: Confocal microscopic analyses of hair cell formation and organization in the three cristae, the first three neuromasts, and the utricular macula of WT siblings and *rbm24a* mutants under the *Tg(pou4f3:GAP-GFP)* transgenic background. The cristae and neuromasts were imaged at 3 dpf, and the maculae at 2 dpf. Arrow indicates a cell extruded from the utricular macula while remaining connected to a hair cell through a cytoplasmic bridge. Scale bar: 10 μm. **H**: Statistical analyses compare the presence of kinocilia in the three cristae between WT siblings and *rbm24a* mutants. All kinocilia were counted regardless of their height. The number in each column indicates total embryos scored from three independent experiments (***, $p < 0.001$; Student's *t*-test). **I**: Statistical analyses of the proportion of utricular maculae with cell trailing. Numbers in the stacked columns indicate total embryos scored from three independent experiments. **J**: Statistical analyses of total hair cells present in the first three neuromasts. The results were obtained from three independent experiments with total numbers of embryos indicated in the columns (***, $p < 0.001$; Student's *t*-test). **K**: In situ hybridization analysis shows the expression of *rbm24a* transcripts in the otic vesicle and the pLLP at 1 dpf. In addition to the lens and heart, the hybridization signals are also detected in the anterior crista (aC) and posterior crista (pC), and in the pLLP. A trailing area between the pC and the pLLP can be also distinguished, which corresponds to the formation of the pLLP form the caudal region of the otic vesicle. The embryo is oriented with anterior up and dorsal on the right. Scale bar: 50 μm.

Supplementary Data

Materials and Methods

Zebrafish

Adults of the AB strain were maintained in standard housing systems (Haisheng), and early embryos were cultured at 28.5°C in a temperature-controlled incubator. The *rbm24a* mutant line was generated using TALEN genome-editing technique as recently described (Shao et al. 2020). Heterozygous carriers were crossed with the *Tg(pou4f3:GAP-GFP)* transgenic zebrafish (Xiao et al. 2005). Homozygous mutants could be distinguished by the presence of heart edema at 1.5 dpf onward, and the genotype was subsequently verified by allele-specific PCR using specific primers (Fig. S1) as described previously (Xing et al. 2018). To prevent pigment development in some experiments, embryos at 1 dpf were cultured in the presence of 50 mM phenylthiourea (Sigma Aldrich).

Startle response test

WT and mutant embryos at 3 dpf were placed individually in a well of 24-well plate with 1 mL of embryo medium (Westerfield, 2007). Their behaviors were recorded using the EthoVision XT Version 9.0 System (Noldus, Netherlands) for a short period of 6 seconds. A pure-tone acoustic stimulus (500 Hz, 80 dB) was delivered at 3.5 seconds using the SweepGen software, and the swimming speed of embryos was monitored using an infrared detector. Each embryo was tested 15 times, with an interval of 5 minutes. The experiments were performed using three independent batches of embryos, and the results were expressed as the percentage response manifested by a single embryo.

Quantification of otic vesicle size

WT siblings and mutant embryos were cultured at 28.5°C. At appropriate stage, they were embedded in 1% low melting agarose and individually imaged at the otic vesicle under confocal differential interference contrast mode. The otic vesicle from each image was analyzed using ImageJ software (NIH Image), and the otic size was determined by calculating the number of pixels using at least three embryos in each condition.

In situ hybridization

A short region within the coding sequences of different genes was amplified by PCR from embryonic cDNAs, and cloned in pGEM-T easy vector (Promega). The plasmids were linearized using appropriate enzymes, and antisense probes were synthesized in the presence of digoxygenin-labeled rNTP mix (Roche Diagnostics). Embryos were fixed in 4% paraformaldehyde at 4°C overnight and stored in methanol. In situ hybridization was performed using published protocol (Westerfield, 2007), and BM purple (Roche Diagnostics) was used as a substrate of alkaline phosphatase.

Confocal microscopy

Live embryos were anesthetized in tricaine solution (0.17 $mgmL^{-1}$) and embedded in a cavity microscope slide with 4% methylcellulose. Live Images of whole embryos were acquired using a fluorescence microscope (Leica, M205FA), and hair cells were examined under a confocal microscope (Lecia, SP5 II). Z-stack projections were obtained by using the z-projection function.

Statistical analyses

The data were obtained from at least three different batches of embryos, with representative images shown. Statistical analyses were performed using unpaired Student's *t*-test and GraphPad Prism 6 software, with *p* values indicated in both the figures and the corresponding figure legends.

References

Shao, M., Lu, T., Zhang, C., Zhang, Y.Z., Kong, S.H., Shi, D.L., 2020. Rbm24 controls poly(A) tail length and translation efficiency of crystallin mRNAs in the lens via cytoplasmic polyadenylation. Proc. Natl. Acad. Sci. U. S. A. (in press).

Westerfield, M. 2007. The zebrafish book: a guide for the laboratory use of zebrafish (Danio rerio), Fifth Ed. University of Oregon Press.

Xiao, T., Roeser, T., Staub, W., Baier, H., 2005. A GFP-based genetic screen reveals mutations that disrupt the architecture of the zebrafish retinotectal projection. Development 132, 2955-2967. https://doi.org/10.1242/dev.01861.

Xing, Y.Y., Cheng, X.N., Li, Y.L., Zhang, C., Saquet, A., Liu, Y.Y., Shao, M., Shi, D.L., 2018. Mutational analysis of dishevelled genes in zebrafish reveals distinct functions in embryonic patterning and gastrulation cell movements. PLoS Genet. 14, e1007551. https://doi.org/10.1371/journal.pgen.1007551.

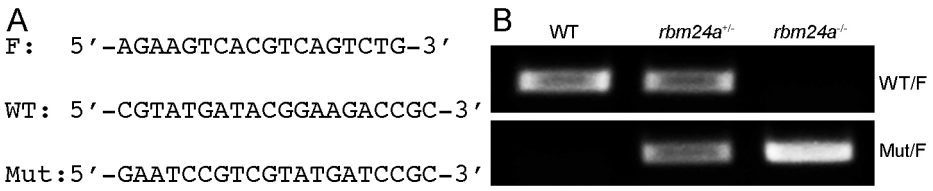

Fig. S1. Genotyping using allele-specific PCR. **A**: Primer sequences. **B**: PCR products amplified by different primer combinations, using genomic DNA from WT siblings, and heterozygous and homozygous *rbm24a* mutants.

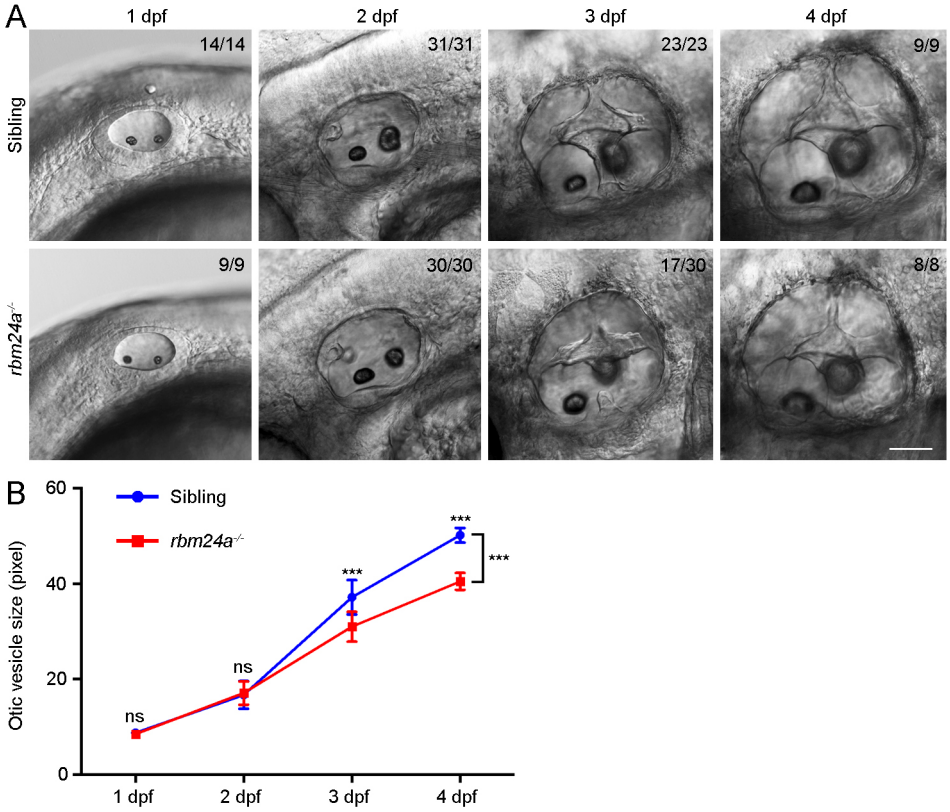

Fig. S2. Delayed growth of otic vesicles in *rbm24a* mutants. **A**: Confocal differential interference contrast images show otic development in WT siblings and *rbm24a* mutants from 1 to 4 dpf. Numbers in the denominator in each image were used for statistical analyses. Scale bar: 50 μm. **B**: Statistical analyses compare the size of otic vesicles between WT siblings and *rbm24a* mutants (ns, not significant; (***, $p < 0.001$; Student's *t*-test).

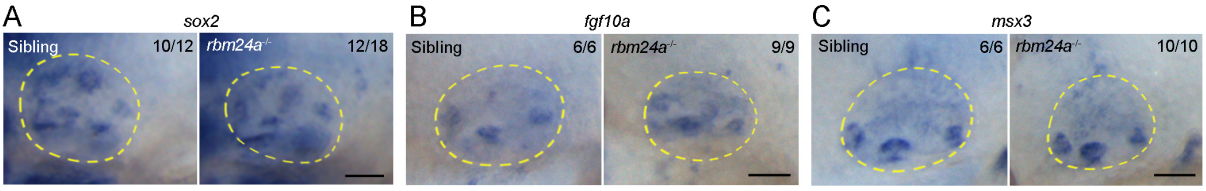

Fig. S3. Expression of otic vesicle markers in WT siblings and *rbm24a* mutants at 3 dpf. **A**: Expression of *sox2*. **B**: Expression of *fgf10a* in the cristae. **C**: Expression of *msx3* in the cristae. Scale bars: 25 μm.